Immobilizing chromate reductase NfoR on magnetic biochar reduced Cr(VI) in copper-containing wastewater

Immobilizing chromate reductase NfoR on magnetic biochar reduced Cr(VI) in copper-containing wastewater

Huawen Han[a,#], Peizhi Song[a,#], Zhuoshan Cai[b], Weijun Dong[a], Aman Khan [a], Ke Yang[d], Yitian Fang[e], Pu Liu[a], Ondřej Mašek[c,*], Xiangkai Li[a,*]

[a] Ministry of Education Key Laboratory of Cell Activities and Stress Adaptations, School of Life Science, Lanzhou University, Tianshui South Road #222, Lanzhou, Gansu 730000, PR China

[b] College of Grassland Science, Gansu Agricultural University, Lanzhou 730070, Gansu 730000, PR China

[c] UK Biochar Research Centre, School of GeoSciences, University of Edinburgh, Crew Building, King's Buildings, Edinburgh EH9 3FF, United Kingdom

[d] State Key Laboratory of Applied Organic Chemistry, Lanzhou University, Gansu, Lanzhou, 730000, China

[e] State Key Laboratory of Microbial Metabolism, School of Life Sciences and Biotechnology, Shanghai Jiao Tong University, Shanghai 200240, China

[#]These authors contributed equally to this work.

* Corresponding author:

Xiangkai Li, Ph.D.

Phone: +86-931-8912560

Fax: +86-931-8912561

E-mail: xkli@lzu.edu.cn

Abstract

Heavy metals (e.g. copper) in smelting wastewater inhibited microbial Cr(VI) reduction, previous report found that a novel chromate reductase NfoR exhibited Cu(II)-enhanced activity and broad-

spectrum metal tolerance. In this study, magnetic biochar (MB) from pine sawdust was fabricated to immobilize NfoR via covalent binding. MB-NfoR showed a 2.6- and 2.1-folds higher activity in reducing Cr(VI) to Cr(III) compared to free NfoR and MB, respectively. XPS and EPR analysis showed that NfoR catalysis and persistent free radicals (PFRs) are responsible for Cr(VI) reduction mechanism of MB-NfoR. The addition of Cu(II) increased the MB-NfoR activity 2.3-fold compared to that of without Cu(II). The maximum Cr(VI) removal by MB-NfoR in the pure Cr(VI) solution was 98% at 45°C and pH 6.0, and the MB-NfoR retained 68.3% of its initial activity even after five consecutive cycles. Application of MB-NfoR in smelting wastewater can simultaneously remove 94% Cr(VI) and 52.1% Cu(II). Furthermore, treated smelting wastewater by MB-NfoR showed no phytotoxicity and enriched numerous oligotrophic bacteria. This study provides a novel 'one-stop' strategy for decontamination of effluents combined with heavy metals, utilizing synergies offered by constituents in such waste streams.

Keywords: Magnetic biochar; immobilized enzyme; chromate reductase; Cr(VI) reduction; smelting wastewater

1 Introduction

Industrial activities, such as electroplating, metal casting, hydrometallurgy, and mining, generate large amounts of chromium/copper-containing wastewater (Barbosa et al., 2020). It is estimated that 41 million liters of Cr-contaminated tannery wastewater was produced worldwide annually (Younas et al., 2021). These non-biodegradable metals can be accumulated through the food chain (Wu, H. et al., 2019). Among these metals, hexavalent chromium [Cr(VI)] raises great concern due to its mutagenicity and carcinogenicity (DesMarais and Costa, 2019). Conventional processes to reduce toxic metals involve chemical precipitation, flotation, electrocoagulation, ion

exchange, and membrane filtration (Bezzina et al., 2020). However, these methods have their own drawbacks, such as secondary pollution, high cost, low efficiency, and membrane fouling. Thus, the treatment of such mixed chromium/copper-containing wastewater requires new solutions.

Reduction of highly toxic Cr(VI) to less toxic Cr(III) by microorganisms is a promising alternative for the cleanup of combined heavy metal pollution *via* reduction or adsorption, due to its efficacy, eco-friendliness, and low costs (Tan et al., 2020). Various Cr(VI)-reducing bacteria have been isolated with a maximum tolerance to 800 $mg \cdot L^{-1}$ Cr(VI) (He et al., 2009), such as *Oceanobacillus oncorhynchi* (Zeng et al., 2019), and *Bacillus sp.*(Tan et al., 2020). In most cases, chromium pollution exists in the form of combined heavy metals. The majority of heavy metals (e.g. Co, Zn, Cd, Cu) inhibited microbial Cr(VI) reduction (Dey and Paul, 2012; Tan et al., 2020). Some metallurgical/electroplating wastewater effluents with high concentration of copper also preclude the performance and direct application of Cr(VI)-reducing bacteria for their treatments (de Morais Nepel, 2020), especially within oligotrophic condition (Ma et al., 2021). Therefore, it is essential to explore novel strategies for the removal of combined heavy metals in metallurgical/electroplating wastewater.

Enzyme immobilization has attracted interest due to its universal applicability, low leaching, enhanced activity, and reusability (Hu et al., 2018). Diverse materials, such as biochar (Han et al., 2019), hydrogels (Xu et al., 2021), and mesoporous silica (Kumar, 2019), have been tested as candidate solid supports for enzyme immobilization. Among them, biochar possesses moderate surface area and abundant functional groups relevant to enzyme loading (Zhang and Hay, 2020). Increasing studies focused on biochar-immobilized laccase for the degradation of carbamazepine

(Naghdi et al., 2017), anthracene (Imam et al., 2021), diclofenac (Lonappan, 2018), and bisphenol A (Zhang, Y. et al., 2020); The role of biochar-immobilized lipase (Cea et al., 2019) and biochar-immobilized cellulase (Mo et al., 2020) have been less explored. However, the treatment of combined heavy metal pollution driven by biochar immobilized chromate reductase remains unclear.

Recent studies highlighted the potential of magnetic biochar for environmental remediation due to its high adsorption capacity and separation performance (Zhang, R. et al., 2020; Zhang et al., 2021), as well as the degradation of organic pollutants and Cr(VI) reduction via persulfate activation and Fenton-like reaction (Wen et al., 2022). For example, the presence of Fe_3O_4 and persistent free radicals (PFRs) in magnetic biochar induced a synergistic effect on Cr(VI) reduction (Zhong et al., 2018). Recent studies have not focused on the role of PFRs of biochar-immobilized enzyme in the degradation of tested pollutants. In this regard, magnetic biochar immobilized chromate reductase can benefit from the Cr(VI) reduction in copper-containing wastewater via synergistic effect.

Our previous studies reported that a new clade of chromate reductase NfoR from *Staphylococcus aureus* exhibited Cu(II)-enhanced activity and broad-spectrum metal tolerance (Han et al., 2021). In this study, we covalently immobilized chromate reductase NfoR on magnetic biochar (MB) and raw biochar (RB) for treating smelting wastewater utilizing synergies offered by constituents. The immobilized NfoR's contributions to Cr(VI) removal are quantified in comparison with free enzyme NfoR and explored the Cr(VI) removal mechanism of MB-NfoR. Various governing parameters were optimized to improve the performance of MB-NfoR. Also, Michaelis-Menten kinetics of immobilized NfoR and reusability for Cr(VI) removal were explored. After adding MB and immobilized NfoR, microbial community evolution and Cr(VI) removal rate in

smelting wastewater were examined. Additionally, the phytotoxicity of treated smelting wastewater was also investigated to assess any potential remaining environmental risks. This study provides a new insight on the decontamination of smelting wastewater by utilizing magnetic biochar immobilized chromate reductase.

2 Materials and methods

2.1 Purification and enzyme assays of NfoR and laccase CueO

The purification procedure and enzyme assays of chromate reductase NfoR and laccase CueO were reported as previously (Han et al., 2021). The effects of pH, temperature and metal on NfoR activity were also evaluated, respectively. The detailed information and chemical reagents used in this study were presented in Supporting Information (SI).

2.2 Fabrication of raw and magnetic biochar

Four kinds of biomass, including pine needle (PN), reed straw (RS), pine sawdust (PS), and manchurian ash (MA), were crushed using a pulverizer and sieved through a 200-mesh. The resultant powders were pyrolyzed in a tube furnace (OTF-1200X, China) under N_2 conditions and held at peak temperatures of 400–500°C for 2 h before cooling naturally. The resultant biochars were PNB400, PNB500, RSB400, RSB500, PSB400, PSB500, MAB400, and MAB500 based on their pyrolysis temperatures. According to the characteristics of these raw biochars, magnetic biochar (MB) was prepared by dissolving 10 g PS in a 60 mL $FeCl_3$ solution (0.5 $M \cdot L^{-1}$) and stirring continuously for 2 h. After drying for 2 h in the oven, the mixture was pyrolyzed using a gas flow-controlled tube furnace maintained at 600°C with a 10°C·min^{-1} heating rate for 2 h under N_2 atmosphere. The resultant MB was collected by vacuum filtration and then dried for 24 h at 28°C.

2.3 Immobilization of NfoR on raw and magnetic biochar

For stable immobilization of NfoR on the raw and magnetic biochar, chromate reductase NfoR (1 $g \cdot L^{-1}$) was incubated in 20 mM Tris-HCl solution (pH 8.0) containing biochar (75 $g \cdot L^{-1}$), followed by the addition of 50% glutaraldehyde (at a final concentration of 3%) for crosslinking enzymes at 16°C. After 2 h of covalent immobilization, the produced raw biochar-immobilized NfoR (RB-NfoR) and magnetic biochar-immobilized NfoR (MB-NfoR) were centrifuged at 6000 *g* for 30 min, and discarded the supernatant. Subsequently, RB-NfoR and MB-NfoR were washed three times using the same pH buffer to remove excessive reagent and freeze-drying for 36 h in the lyophilizer. The final samples were stored at 4°C for further use. For non-enzyme treatment, the same process was followed except that the enzyme was omitted. The immobilization rate of RB-NfoR and MB-NfoR was measured by Brandford method.

2.4 Performance, optimization and reusability of biochar-immobilized NfoR in Cr(VI)solution

Briefly, 0.01 g MB-NfoR was used to remove Cr(VI) (final concentration of 200 μM) in Tris-HCl buffer containing 300 μM NADH solution by shaking at 200 rpm for 30 min. Under the same conditions, supplementation of RB-NfoR in enzyme reaction was positive control while MB and free NfoR were negative controls, respectively. The residual Cr(VI) concentration in the supernatant was measured utilizing diphenyl carbazide (DPC) method as previously described (Han et al., 2017). In addition, considering Cu(II)-enhanced NfoR activity, the effect of Cu(II) on the activity of MB-NfoR was also evaluated. Enzyme activity measurement was similar to that of the previous method.

To improve the performance of immobilized NfoR, the effects of various parameters on the performance of RB-NfoR and MB-NfoR were detected, including reaction time (2.5–60 min), pH

(6.0-10.0), temperature (16-45°C), and the dose of immobilized NfoR (5–15 $g \cdot L^{-1}$). Subsequently, the Michaelis–Menten kinetics for immobilized-enzyme (MB-NfoR, RB-NfoR) was calculated in various Cr(VI) concentration (100–400 μM) as previously described in free NfoR (Han et al., 2021)

The reusability of biochar-immobilized NfoR was also investigated by recovering the immobilized NfoR via centrifugation and re-suspending it into a fresh reaction buffer as described previously (Zhang and Hay, 2020). In each cycle, 0.01 g of MB-NfoR or RB-NfoR was reacted with 200 μM Cr(VI) supplemented with 300 μM NADH at 45°C for 30 min. After centrifugation, the supernatant was used to detect the Cr(VI) reduction rate. The residual MB-NfoR was freeze-dried in a vacuum and then supplemented with fresh Cr(VI) solution, NADH and Tris-HCl buffer for reusability.

2.5 Smelting wastewater treatment by biochar-immobilized NfoR

To investigate the performance of biochar-immobilized NfoR in smelting wastewater, the tested water sample was collected from the smelting plant of Baiyin City, Gansu Province, China. The concentration of various metals (e.g. Cu, Zn, Cr, Cd, Mn, As, Pb) were presented in supporting information. Before the addition of the immobilized enzyme, smelting wastewater water was spiked with 600 μM sodium acetate as electron donor of Cr(VI) reduction catalyzed by NfoR. Subsequently, 10 $g \cdot L^{-1}$ of MB, RB-NfoR and MB-NfoR was added into 1L smelting wastewater, respectively. All treatments were shaking for 12 days to remove the combined heavy metals at 37°C. Afterward, the residual Cr(VI) and other divalent metals were measured and the measurements were performed in triplicate.

2.6 Sample collection, DNA extraction and processing for sequencing

To explore the effect of biochar and immobilized NfoR on the microbial community of smelting wastewater, four groups of smelting wastewaters, such as CK (without adding biochar or immobilized enzymes), MB, RB-NfoR and MB-NfoR, were collected after 12 days as previously described (Calderón-Franco et al., 2021). Briefly, 600 mL wastewater of each group was filtrated using a 0.22 μm membrane to collect the microbes. Each membrane was cut into several pieces by use of a sterile scissor and was stored separately in a sterile centrifuge tube. Subsequently, each tube was stored immediately in liquid nitrogen until DNA extraction.

Total genomic DNA was extracted directly by using water sample DNA extraction kit (Omega, Norcross, GA, USA) following the manufacture's instruction. A Qubit 4 fluorometer was used to determine the concentration of total DNA, and 1% gel electrophoresis was selected to check the integrity of the obtained DNA. The 16S rRNA gene V4-V5 variable region was amplified using primers 515F-806R. Then PCR products were subsequently determined on the platform at Illumina Miseq platform by Genesky Biotech (Shanghai, China). After removing barcodes and primers, and further cleaning chimera, short sequences through QIIME (v1.8.0, http://qiime.org/), the obtained high-quality sequences were clustered into operational taxonomic units (OTUs) with a 97% sequence similarity threshold using Uclust. Data analysis was performed using Genesky Cloud (http://cloud.geneskybiotech.com).

2.7 Toxicity analysis of biochar- and immobilized NfoR-treated wastewater

Phytotoxicity of biochar- and immobilized NfoR-treated smelting wastewater were tested using a five-day "all exposure route" alfalfa (*Medicago sativa*) seed germination test, respectively. The deionized water was chosen as a control. Fifty alfalfa seeds were placed in one Petri dish (90 mm

diameter) on a filter paper moistened with deionized water. Subsequently, 20 mL of deionized water or treated wastewater was added to the Petri dishes in three replicates. All Petri dishes were covered and incubated in the dark at 25°C ± 0.5°C for five days, and then the germination rate, seedling length, and root length were recorded, respectively.

2.8 Analytical methods

Cr(VI) concentrations in the samples were measured spectrophotometrically using diphenyl carbazide (DPC) method at a wavelength of 540 nm (Li et al., 2020). The morphological features of biochar and biochar-immobilized enzymes were characterized using scanning electron microscopy (S-3400N, Hitachi, Japan). The BET surface area, the total pore volume and the average pore diameter of the RB-NfoR and MB-NfoR were investigated with N_2 adsorption-desorption measurements at 77 K using an automated surface area analyzer (TristaII 3020, America). Thermogravimetric analysis (TGA) was conducted in an N_2 atmosphere using a STA 449 F3 simultaneous DSC-TGA. The temperature was increased by 20 °C per minute between 25 and 800 °C. X-ray diffraction (XRD) was used to detect the phase composition of RB-NfoR and MB-NfoR using a Rigaku diffraction spectrometer (Ultimate IV, Japan) equipped with Cu Ka target 40 kV/40 mA X-ray source over the 2θ range of 10–80°. The hysteresis curves of MB and MB-NfoR were measured by vibrating sample magnetometry (VSM) (EV9, MicroSence, USA). ICP-MS (PE, Avio 500) was used to detect the metal concentrations in smelting wastewater.

To explore the removal mechanism of biochar-immobilized NfoR, the functional groups of immobilized NfoR before and after Cr(VI) removal were characterized by Fourier-transform infrared spectroscopy (FTIR) (Nicolet 670, USA) with a scanning spectrum range of 500 cm^{-1} –

4000 cm^{-1}. The formed Cr(III) adsorbed onto the MB-NfoR and RB-NfoR was quantified after separating the supernatant by X-ray photoelectron spectroscopy (XPS) (Krotas, England). Meanwhile, free radicals quenching experiments of RB-NfoR and MB-NfoR were conducted using spin-trap reagent DMPO in Tris-HCl (Yi et al., 2020b), and the outcome of •OH was measured with a fluorescence spectrophotometer (Hitachi, Japan, F-4600). The intensity of PFRs in RB-NfoR and MB-NfoR was measured by an electron paramagnetic resonance spectrometer (EPR, EMXmicro-6/1/P/L, Bruker, Karlsruhe Germany), and its operating parameters were described as previously (Tang et al., 2021).

2.9 Statistical analysis

All collected data were analyzed in SPSS v.20.0. Turkey's comparison was used for statistics comparison, and a significant difference considered when *P* value was below 0.05.

3 Results and Discussion

3.1 Enhanced NfoR activity supplemented with Cu(II)

Our previous studies found that a novel chromate reductase NfoR was involved in Cu(II)-enhanced microbial Cr(VI) reduction (Fig. 1A) (Han et al., 2021). The optimum temperature and pH for NfoR activity were 37°C and 6.0 (Fig.1B, Fig.1C). Under pH 4.5, acetate and NADH functioned as electron donors for Cr(VI) reduction, resulting in a maximum Cr(VI) reduction rate (Fig.1 B). Owing to combined heavy metal pollution in industrial wastewater, we further evaluated the adaptability of NfoR supplemented with various metal ions (Fig. 1D). Most metal ions had no impact on NfoR activity except on Cu(II) and Ni(II). The addition of Cu(II) caused a 1.4-fold increase in the relative activity of NfoR. These pieces of evidence indicate that NfoR exhibited

better metal tolerance, and Cu(II)-enhanced NfoR activity benefits from combined heavy metals pollution.

Representative chromate reductases responsible for microbial Cr(VI) reduction were ChrR and YieF (Han et al., 2017). Subsequently, a series of chromate reductases have been characterized, including NfsA, NemA, NhaG , CsrF, NitR, and NfoR (Han et al., 2021). These chromate reductases transfer electrons from NAD(P)H to Cr(VI) *via* flavin mononucleotide (FMN) or flavin adenine dinucleotide (FAD). The opposite phenomena were observed in the partial purification of chromate reductase from a novel *Ochrobactrum* sp. strain Cr-B4 (Hora and Shetty, 2015). In our studies, NfoR showed Cu(II)-enhanced activity because a dual-channel electron transfer of NfoR via Cu(II) and FMN accelerates the electron transfer (Han et al., 2021), as well as wide-spectrum metal tolerance. These observations suggested that NfoR has a wide application prospect.

3.2 Fabrication and characterization of biochar-immobilized NfoR

The selection of functional support material prior to enzyme immobilization is of great concern for enzyme activity and stability (Naghdi et al., 2017). Four kinds of biochars, derived from pine needle (PN), reed straw (RS), pine sawdust (PS), and manchurian ash (MA), were chosen as candidate supporting materials of NfoR (Fig. S1). Among these, pine needle biochar (PNB) and reed straw biochar (RSB) possessed abundant –C=O and C-H functional groups (Fig. S2). However, these biochars exhibited a low immobilization rate of NfoR (below 30%) *via* adsorption (Fig. S3). To improve the immobilization efficiency of NfoR, magnetic-modified PS biochar (MB) was fabricated for covalent immobilization of NfoR by using 3% glutaraldehyde (Fig. 2A); whereas covalent immobilization of NfoR on raw biochar (RB) from PS was chosen as a positive control.

After magnetic modification, magnetic particles were distributed on the surface of MB (Fig. 2B). NfoR loaded on biochars showed an obvious change in the surface texture of MB and RB, which is similar with modified magnetic biochar nanoparticles supported tyrosinase (He et al., 2020). In contrast, almond shell biochar-immobilizing laccase only clumped biochar without changing its surface texture(Lonappan, 2018). The BET specific surface area of MB-NfoR (25.0 $m^2 \cdot g^{-1}$) was larger than that of RB-NfoR (1.10 $m^2 \cdot g^{-1}$) (Fig. 2C), which was one order of magnitude lower than Mn doped magnetic biochar (Huang et al., 2020). The pore distribution of MB-NfoR mainly ranged from 2 nm to 30 nm (Fig. S6), this layered porous structure accelerated the catalytic reaction of pollutants. TGA-DSC analysis showed that the MB-NfoR was more thermally stable than RB-NfoR (Fig. S7), with a mass loss of 15% up to 800℃ under N_2 condition.

The FTIR spectra of MB and RB showed a sharp peak at approximately 1160 cm^{-1}, 1598 cm^{-1}, and 3420 cm^{-1} corresponding to C-H, C=O, and O-H stretching, respectively (Fig.2D). After NfoR immobilization, a decrease in the intensity of the bands at approximately 3420 cm^{-1}, 1598 cm^{-1}, 1500 cm^{-1} and 1160 cm^{-1} suggested that the NfoR binded to functional groups of MB and RB via crosslinking. Furthermore, four bands appeared at 1564 cm^{-1}, 1050 cm^{-1}, 773 cm^{-1}, and 607 cm^{-1}, due to the probable additional groups of NfoR (Imam et al., 2021). This phenomenon was distinct from magnetic biochar-immobilized laccase; a dative bond between the iron of MB and laccase was formed, causing an additional C=O stretching at 1700 cm^{-1} (Zhang and Hay, 2020). Although functional groups of MB and RB exhibited a minor difference, MB achieved a 100% immobilization rate of NfoR (Fig. S4). A similar phenomenon was observed in acid modified pinewood biochar-immobilized laccase (Naghdi et al., 2017). Citric acid modified biochars provided abundant COOH

groups and available surface area, resulting in a 16–20% improvement in laccase binding (Lonappan, 2018).

The XRD patterns of MB-NfoR and RB-NfoR exhibited clear differences between the two materials (Fig.2E). The peak at around 25°, representing amorphous C atoms, indicated that the crystallinity of RB-NfoR was higher than that of MB-NfoR (Huang et al., 2020). Several peaks of MB-NfoR at around 18°, 30°, 35°, 43°, 57°and 62° corresponded to planes of Fe_3O_4 (Fig.2E), which agreed well with the result of VSM analysis (Fig. S5). Covalent immobilization of NfoR showed a negligible impact on the magnetic intensity of MB. The signals of FeO and Fe_2O_3 were not detected in MB-NfoR, which is inconsistent with other magnetic biochars (Yi et al., 2020c)

3.3 Immobilized NfoR on magnetic modified biochar enhanced Cr(VI) removal

To further probe the performance of immobilized NfoR, we detected the Cr(VI) removal rate of MB-NfoR using RB-NfoR as a positive control (Fig. 3A). MB-NfoR exhibited a 2.7-, 2.1-, and 2.3-folds increase in Cr(VI) removal compared to free NfoR, MB and RB-NfoR (P<0.001). The Cr(VI) removal rate of MB-NfoR reached up to 88.7%. The presence of Cu(II) increased the relative activity of MB-NfoR up to 2.3 times compared to the treatment in the absence of Cu(II) (Fig.3B). This is ascribed to Cu(II)'s role as a cofactor of NfoR (Han et al., 2021). To confirm this, laccase CueO with Cu(II)-enhancement was also immobilized on magnetic biochar (MB-CueO), supplementation of Cu(II) significantly enhanced the specific activity of MB-CueO after 2, 2′-azino-bis (3-ethylbenzothiazoline-6-sulphonic acid) (ABTS) oxidation (Fig. S8). These findings indicated that Cu(II)-enhanced enzymes have excellent application potential in combined pollution remediation.

FTIR spectra of immobilized NfoR before and after Cr(VI) removal was shown in Fig. 3C and Fig. 3D. As for MB-NfoR, the intensity of the peaks around 3400 cm^{-1}, 2900 cm^{-1},1637 cm^{-1}, 1538 cm^{-1}, 1152 cm^{-1}, and 573 cm^{-1} was weakened after reaction. This indicates that substances containing –OH group, $–CH_2$ group, aromatic C=C/–C=O groups, C-O-C groups and Fe-O variations are associated with the Cr(VI) removal (Yi et al., 2020c). In contrast, FTIR spectra of RB-NfoR showed mainly C-O-C groups and –C=O stretching vibration (Fig. 3C). Furthermore, the XRD patterns of RB-NfoR before and after Cr(VI) removal appeared several new peaks at 25°, 28°, 38°, and 47° (Fig. 3E), possibly due to Cr(VI) adsorption or reduction. In case of MB-NfoR, the main signal peaks were retained after reaction, suggesting that MB-NfoR possesses excellent stability (Fig. 3F). However, a slight peak shift was observed and the intensity also decreased (Fan et al., 2022), which can be attributed to the Cr(VI) removal. Moreover, the BET surface area and pore volume of MB-NfoR after Cr(VI) removal decreased to 13.32 $m^2 \bullet g^{-1}$ and 0.032 $cm^2 \bullet g^{-1}$ (Fig. S9), only accounting for 53.3% and 47.3% of the fresh MB-NfoR, respectively. These findings further confirm high Cr(VI) removal capacity of MB-NfoR.

Our observations revealed that MB-NfoR offers an absolute advantage over free NfoR. This enhanced Cr(VI) removal may be attributed to adsorption and PFRs-mediated Cr(VI) reduction of magnetic biochar (Tang et al., 2021; Zhong et al., 2018), e.g. The Fe_3O_4 and carbon-centered PFRs of magnetic biochar contributed to ~81.8% and ~18.2% of total Cr(III) generation. Similar results were obtained for biochar-immobilized laccase, which displayed higher activity than free laccase in the removal of anthracene and carbamazepine (Imam et al., 2021; Naghdi et al., 2017). Cage-like 3D channel structure of the hydrogels-immobilized HRP (horse radish peroxidase) also maintained

higher activity than observed in free enzymes (Yang et al., 2019). However, porous biochar/chitosan composites immobilized cellulase showed controversial results (Mo et al., 2020), as the supported cellulase only retained 67 % of the activity of free cellulase. More importantly, the Cr(VI) removal of MB-NfoR is superior to that of RB-NfoR, which was similar to results of MB-laccase (Zhang and Hay, 2020), where the maximum activity of MB-laccase was 3.7 times higher than that of RB-laccase (8.8 U/mg support). This suggests that functionalized biochar can be promising support material for enzyme immobilization. Although multiple heavy metals [e.g. Cd (II), Pb(II), and Zn (II)] present in smelting wastewater inhibited the activity of chromate reductase (Hora and Shetty, 2015), Cu(II)-enhanced MB-NfoR activity can overcome these issues owing to its broad-spectrum metal tolerance.

3.4 Potential mechanism of Cr(VI) removal

To further study the fate of Cr(VI) in the solution, the formed Cr(III) by NfoR catalysis haven't been detected in the supernatant because the Cr(III) complexes may be adsorbed on the surface of MB-NfoR. XPS was used to examine the elemental composition of MB-NfoR and RB-NfoR after the Cr(VI) removal (Fig. 4). Typical Cr XPS peaks appear in the total survey spectra of MB-NfoR and RB-NfoR (Fig. 4A). The C1s spectra of MB-NfoR revealed the presence of three component peaks (Fig. 4B), corresponding to C-C groups (284.8 eV), C-O-C groups (286 eV) and O-C=O groups (288.5 eV), respectively. The C1s binding state of MB-NfoR showed higher relative percentage of C-O-C and O-C=O groups due to magnetic modification (i.e. 29.97% and 32.25% for MB-NfoR versus 13.46% and 24.44% for RB-NfoR). Moreover, two distinct peaks at 576.0–578.0 eV ($Cr2p_{3/2}$) and 586.0–588.0 eV ($Cr2p_{1/2}$) were observed in MB-NfoR and RB-NfoR (Fig.4C), but

Cr(VI)-O was not detected (Yang et al., 2021). This indicates the formation of Cr_2O_3 and $Cr(OH)_3$ precipitates after Cr(VI) reduction (Diao et al., 2018; He et al., 2021). High-resolution of Fe2p spectra existed two valence states of iron species on MB-NfoR after Cr(VI) removal (Fig. 4D). The peaks at 710.71 and 723.82 eV corresponded to the binding energies of Fe_2O_3 (Diao et al., 2016; Huang et al., 2020); whereas the peaks at 713.06 and 726.28 eV are associated with FeO (Yang et al., 2021). After the reaction, the percentage of FeO in MB-NfoR only slightly decreased 0.6%. This showed that the iron oxides are not involved in the Cr(VI) removal.

The XPS spectra revealed that Cr(III) is the only form of MB-NfoR-Cr (Fig. 4C), this can't explain why the MB-NfoR exhibited 2-fold higher Cr(VI) reduction than that in free NfoR (Fig. 3A). Existing studies reported that PFRs of biochar can function as electron donor and electron shuttle for Cr(VI) reduction (Xu et al., 2019; Zhu et al., 2020), thus we speculated that the presence of PFRs also played role in Cr(VI) reduction by MB-NfoR. To validate this hypothesis, EPR spectra were used to identify reactive species existing in MB-NfoR and RB-NfoR system by using DMPO and TEMP as trapping agents, respectively (Fig. 4E). As expected, three PFRs, such as •OH, $•O_2^-$ and $^1O_2$, were observed in MB-NfoR; whereas RB-NfoR system only detected •OH and $^1O_2$ formation due to its inherent low PFRs concentration (Wang et al., 2020). Among these PFRs, •OH and $^1O_2$ participated in the degradation refractory organic pollutants from water environments (Han et al., 2022) while solution $•O_2^-$ was responsible for Cr(VI) reduction of biochar (Chen et al., 2021). These evidences suggested that the presence of $•O_2^-$ in MB-NfoR promotes the Cr(VI) reduction.

Our findings revealed that the Cr(VI) removal mechanism of MB-NfoR derived from both the reduction of immobilized NfoR and PFRs (Fig. 5), accounting for 52.6% and 47.4%, respectively

(Fig. 3A). Studies in L-MBC (laccase immobilized magnetic biochar) and pinewood biochar immobilized laccase indicated adsorption and enzymatic degradation were the main mechanisms of bisphenol A (BPA) and carbamazepine removal, respectively (Naghdi et al., 2017; Zhang, Y. et al., 2020). These studies did not discuss the role of PFRs in the degradation of organic pollutants of biochar-immobilized laccase. Despite the lack of biochar immobilized enzymes for heavy metal removal, existing studies found that adsorption and PFRs-mediated Cr(VI) reduction are dominant mechanisms for Cr(VI) removal on magnetic biochar (Tang et al., 2021), and the presence of Fe^0 and Fe_3O_4 can provide active sites for Cr(VI) reduction (Wang et al., 2020). However, XPS of MB-NfoR before and after Cr(VI) removal did not show the characteristic peak of Fe^0 and Fe_3O_4, along with stable FeO intensity, thus eliminating Cr(VI) reduction catalyzed by iron oxides as a potential mechanism (Dong et al., 2021; Yan et al., 2021). Notably, extensive studies only reported singlet EPR signal of magnetic biochar and detected their PFRs concentrations (Tang et al., 2021; Wang et al., 2020), our study confirmed that three types of free radicals (e.g. •OH, $•O_2^-$, $^1O_2$) were present in MB-NfoR and $•O_2^-$ was responsible for Cr(VI) reduction of MB-NfoR. Collectively, these results revealed that Cr(VI) removal of MB-NfoR was reduced to Cr(III), and adsorbed on the surface of MB.

3.5 Optimization of immobilized NfoR and their reusability

To achieve the maximum Cr(VI) reduction of MB-NfoR, the effects of reaction time, pH, temperature, dose of immobilized NfoR, and initial Cr(VI) concentration on the performance of RB-NfoR and MB-NfoR were evaluated (Fig.6). The optimum reaction time for RB-NfoR and MB-NfoR was 30 min, and their corresponding Cr(VI) reduction capabilities were 38.4% and 89.2%,

respectively (Fig. 6A). After immobilization, the optimal pH did not change compared with those of free NfoR (Fig. 6B, Fig. 1C). The highest Cr(VI) reduction of MB-NfoR was 98% at pH 6.0. In contrast to free NfoR (Fig. 1B), MB-NfoR and RB-NfoR showed a wide temperature tolerance of 30–60ºC (Fig. 6C), in accordance with the MB immobilized laccase that retained high activity at 70ºC (Zhang, Y. et al., 2020). Furthermore, high dose of MB-NfoR (15 $g \cdot L^{-1}$) completely exhausted Cr(VI) (Fig. 6D). These results indicates that magnetic MB-NfoR showed higher catalytic activity and better adaptability (Zhang and Hay, 2020). As for steady-state kinetics of immobilized NfoR, the V_{max} of NfoR on MB (88.64 $\mu M \cdot min^{-1}$) was 2.3-fold higher than that of NfoR on RB (38.34 $\mu M \cdot min^{-1}$) (Fig. 6E). The K_m of MB-NfoR (44.27 μM) decreased compared to that of free NfoR (120.84 μM) and RB-NfoR (101.7 μM). Another study by Zhang *et al.* provided detailed information on the enzyme kinetics of MB-bound HRP, an enhanced V_{max} of MB-HRP (1.5 $mM \cdot min^{-1}$) was obtained relative to that of free HRP (1.3 $mM \cdot min^{-1}$) and raw biochar-bound HRP (Zhang and Hay, 2020).

In most cases, loss of activity after one cycle are the main obstacles for large-scale enzyme-catalyzed pollutants remediation (Lonappan et al., 2018). MB-NfoR and RB-NfoR still retained 68.3% and 40% of their initial activities after five cycles of Cr(VI) removal, respectively (Fig. 6F). The decreases in MB-NfoR activity were associated with Fe(III) loss of magnetic biochar. This suggested that immobilizing NfoR into magnetic PS biochar maintains higher activities after repeated use and easy recycling from the reaction mixture. According to Table 1, the reusability of biochar-immobilized enzymes varied within 6%–90%. Such divergence can be ascribed to the tested enzymes, candidate support material and immobilization techniques. Therefore, functionalized

biochar types and immobilized enzymes are crucial factors for manipulating the excellent performance of biochar-immobilized enzyme. Generally, the majority of immobilized enzymes significantly decrease their activities at room temperature owing to the enzyme deactivation, especially pinewood biochar immobilized laccase via adsorption only sustained 6 % of initial activity due to the dissociation of immobilized laccase (Naghdi et al., 2017). Collectively, the fate of immobilized NfoR via covalent immobilization is the loss of NfoR activity.

3.6 Application of immobilized NfoR in smelting wastewater and its toxicity

To evaluate the practical application of MB-NfoR, smelting wastewater was collected from Smelting Plant of Baiyin City, China, containing 800 $mg \cdot L^{-1}$ Cr(VI) and 400 $mg \cdot L^{-1}$ Cu(II) (Fig. S10). After 1 h treatment, the Cr(VI) removal efficiency of MB-NfoR reached 94% (Fig. 7A), which is equivalent to its ability under pure buffer conditions. Furthermore, MB-NfoR can remove 52.1% Cu(II), 10.8% Zn(II), 14.8% Cd(II), 4.2% Mn(II), and 5.8% Pb(II) in smelting wastewater (Fig. 7B). The Cu species in MB-NfoR may exist in the Cu(II)-containing complexes or $Cu(OH)_2$. It has been also reported that aromatic structure and functional groups (e.g. -COOH, -OH) of magnetic biochar can interact with heavy metals to form complexes (Yin et al., 2018). FTIR spectra of MB-NfoR confirmed the presence of abundant aromatic C=C, -OH, C=O groups (Fig.2C, Fig.3D). An obvious difference is in the removal of divalent ions due to the competitive adsorption on MB-NfoR and their initial concentrations (Han et al., 2019). Magnetic biochar has widely been used as an effective adsorbent for removing heavy metals and organic pollutants from wastewater and even from nuclear waste-polluted water (Ye et al., 2020; Yi et al., 2020a). In ultrapure water and secondary effluent, immobilization of laccase on functionalized nanobiochars exhibited an equal carbamazepine

removal rate (Naghdi et al., 2017). However, magnetic biochar-laccase slightly attenuates the BPA removal rate under actual water treatment conditions (Zhang, Y. et al., 2020).

To explore whether biochar- and immobilized enzyme-treated smelting wastewater attained irrigation quality, their toxicity was evaluated *via* the widely used alfalfa growth assays (Fig. 7C). MB-NfoR group shared identical germination rate with H_2O group while the germination rate of alfafa decreased to a half in the treatment of MB and RB-NfoR due to the toxicity of residual Cr(VI) (Fig. 7D). Furthermore, exposure to a MB-NfoR treated wastewater significantly enhanced seedling length and root length compared with H_2O treatments (Fig. 7E–F). Root length in MB-NfoR was 6.59 cm, which was 1.4-, 1.6-, and 1.8-folds higher than that observed in H_2O, MB, and RB-NfoR, respectively. The underlying reason is that MB-NfoR can provide available nutrients for alfalfa growth. Although smelting wastewater still contained other divalent metals after MB-NfoR treatment (Fig. 7B), their low concentrations can stimulate alfalfa growth (Aydinalp and Marinova, 2009). Similarly, magnetic biochar-immobilized laccase exhibited a 10-fold lower acute toxicity toward *Vibrio fischeri* than the previously described carbon-based supports (Zhang and Hay, 2020). Recent studies highlight the formations of toxic contaminants in biochar production, such as polycyclic aromatic hydrocarbons, dioxins, PFRs, and metal cyanide (Luo et al., 2020), with the potential to induce phytotoxicity, ecotoxicity, and cytotoxicity(Han et al., 2022). This study provides strong confirmation that MB is a safe and promising support matrix for enzyme immobilization applications, making it a value-added product from unwanted waste products.

3.7 MB-NfoR enriched the abundance of oligotrophic bacteria of smelting wastewater

To further explore whether the addition of MB and immobilized NfoR influence the microbial

community of smelting wastewater, their microbial community compositions were measured after 12 days by Illumina high-throughput sequencing (Fig. 8). The Shannon index of MB and RB-NfoR was markedly higher than that observed in the control and MB-NfoR groups (P<0.001) (Fig. 8A). As for MB and RB-NfoR, larger specific surface areas accommodate space for more microorganisms, resulting in the richness of microbial communities (Lu et al., 2020). In contrast, the high removal efficiency of MB-NfoR simultaneously decreased the levels of contaminants and nutrients of wastewater, along with low alpha diversity. As for treating of combined heavy metals and dye pollution in wastewater, samples with β-cyclodextrin functionalized biochar amendment exhibited better bacterial community diversity than the corresponding systems under the same environmental pressures but without biochar addition (Wu et al., 2020). Principal coordinate analysis (PCoA) revealed the biochar or biochar-immobilized NfoR significantly altered the microbial community structures of smelting wastewater (Fig. 8B). Samples from the MB-NfoR were far away from those in RB-NfoR and MB, which is consistent with their Cr(VI) removal rate (Fig. 7A).

At the phylum level, the dominant bacterial reads in four groups except MB-NfoR were affiliated to three phyla, including *Proteobacteria* (77.85–99.64%), *Bacteroidetes* (4.42–5.03%), and *Thermi* (2.7–17.43%) (Fig. 8C). RB-NfoR enhanced the relative abundances of *Firmicutes* (3.93%), whereas MB-NfoR lost *Bacteroidetes* and *Thermi* (Fig.8C). At the genus level, the RB-NfoR group was enriched with high abundance of the following genera: *Shewanella* (5.45%), *Pseudomonas* (5.39%), *Bacillus* (3.68%), *Aeromonas* (2.97%), and *Acinetobacter* (2.12%)(Fig.8D). The possible reason is that RB-NfoR treated smelting wastewater still maintains high levels of Cr(VI)

and available nutrients from RB-NfoR stimulate the enrichment of Cr(VI)-reducing bacteria. More important, most bacteria from these genera in RB-NfoR have been proven to possess strong Cr(VI) reduction ability and preserves abundance of Cu(II)-enhanced microbes (e.g. *Bacillus* sp, *Acinetobacter* sp) (Hu et al., 2021; Huang et al., 2019; Mengke et al., 2019; Mohamed et al., 2020; Wu, M. et al., 2019), thus leading to the residual Cr(VI) reduction of RB-NfoR treated wastewater (Han et al., 2021). Distinct from the other three groups, some new genera, such as *Schlegelella* (14.49%), *Silanimonas* (3.14%), and *Lysobacter* (5.92%), sustained high abundance in MB-NfoR group. This change is attributed to the high Cr(VI) removal and Cu(II) removal in MB-NfoR treated smelting wastewater, thus accelerating the enrichment of oligotrophic bacteria of smelting wastewater. These oligotrophic bacteria in MB-NfoR were mainly distributed in oligotrophic habitats (e.g., hot spring), associated with polyhydroxyalkanoates production (Kourilova et al., 2021) and discovery of new antibiotics (de Bruijn et al., 2015).

Collectively, enzyme immobilization has been regarded as a green and sustainable strategy to degrade and transform of pollutants into less toxic or nontoxic form, e.g. immobilized laccases and horseradish peroxidase with the ability to oxidize various types of compounds (Shakerian et al., 2020). Enzyme immobilization has the advantage of better activity than microorganisms for pollution degradation. A growing body of evidence suggests agro-industrial wastes or their value-added products function as potential candidates for enzyme immobilization (Girelli et al., 2020), this contributes to carbon utilization and storage. The key bottleneck of microbial remediation is the treatment of combined pollution, as many toxic pollutants inhibit microbial growth (Liu et al., 2017). As a common pollutant in industrial wastewater, Cu(II) is also an activator or cofactor of most

enzymes (Han et al., 2021). The candidate enzyme NfoR used in this study showed Cu(II)-enhanced activity and broad-spectrum metal tolerance, thus having great potential in the treatment of combined pollution. Immobilizing NfoR on magnetic biochar not only overcomes the drawbacks of chromate reductase in Cr(VI)-containing wastewater, but also exhibited synergistic effects on Cr(VI) reduction by NfoR catalysis and PFRs-mediated reduction. Cr(III) is the only form of MB-NfoR-Cr (Fig. 4C). The treated smelting wastewater by MB-NfoR had no phytotoxicity and increased the abundance of oligotrophic bacteria. This study provides strong evidence that magnetic biochar immobilized chromate reductase is feasible and eco-friendly technology for the treatment of Cr(VI)-containing wastewater.

4. Conclusions

In this research, covalent immobilization of Cu(II)-enhanced chromate reductase NfoR on magnetic biochar was shown to remove up to 94% of Cr(VI), as well as adsorbing 52.1% of Cu(II) in smelting wastewater. NfoR catalysis and PFRs-mediated Cr(VI) reduction are the removal mechanism of MB-NfoR. Regardless of whether it was used in pure buffer or smelting wastewater, MB-NfoR showed a superior performance over RB-NfoR and its relative activity can be further enhanced (more than doubled) in the presence of a common co-contaminant Cu(II). Besides the excellent performance in a one-off use, the MB-NfoR retained 68.3 % of its initial activity after five consecutive use cycles. In addition to the sorption and reduction activity, the RB-NfoR enriched the abundance of some chrome-reducing bacteria in the smelting wastewater, as Cu(II)-enhanced Cr(VI) reduction are common in these bacteria, this contributes to the overall Cr(VI) removal. MB-NfoR group increased the abundance of oligotrophic bacteria (e.g *Schlegelella*, *Silanimonas* and

Lysobacter) and its treated smelting wastewater had no phytotoxicity. This provides a novel and effective strategy for remediation of combined heavy metal pollution.

Acknowledgments

The authors thank the National Natural Science Foundation Grant (No: 31870082, 32070117) and Fundamental Research Funds for the Central Universities grant (No: lzujbky-2019-cd01, lzujbky-2020-pd06). We would like to thank the Central Laboratory of the School of Life Science, Lanzhou University, for providing various instruments and equipment.

References

Aydinalp, C., Marinova, S., 2009. The effects of heavy metals on seed germination and plant growth on alfafa plant (*Medicago sativa*) Bulgarian Journal of Agricultural Science 15(4), 347-350.

Barbosa, R.F.S., Souza, A.G., Maltez, H.F., Rosa, D.S., 2020. Chromium removal from contaminated wastewaters using biodegradable membranes containing cellulose nanostructures. Chemical Engineering Journal 395.

Bezzina, J.P., Robshaw, T., Dawson, R., Ogden, M.D., 2020. Single metal isotherm study of the ion exchange removal of Cu(II), Fe(II), Pb(II) and Zn(II) from synthetic acetic acid leachate. Chemical Engineering Journal 394.

Calderón-Franco, D., van Loosdrecht, M.C.M., Abeel, T., Weissbrodt, D.G., 2021. Free-floating extracellular DNA: systematic profiling of mobile genetic elements and antibiotic resistance from wastewater. Water research 189, 116592.

Cea, M., Gonzalez, M.E., Abarzua, M., Navia, R., 2019. Enzymatic esterification of oleic acid by Candida rugosa lipase immobilized onto biochar. Journal of environmental management 242, 171-177.

Chen, N., Cao, S., Zhang, L., Peng, X., Wang, X., Ai, Z., Zhang, L., 2021. Structural dependent Cr(VI) adsorption and reduction of biochar: hydrochar versus pyrochar. The Science of the total environment 783, 147084.

de Bruijn, I., Cheng, X., de Jager, V., Exposito, R.G., Watrous, J., Patel, N., Postma, J., Dorrestein, P.C., Kobayashi, D., Raaijmakers, J.M., 2015. Comparative genomics and metabolic profiling of the genus Lysobacter. BMC Genomics 16, 991.

de Morais Nepel, T.C., Landers, R., Vieira, M. G. A., & de Almeida Neto, A. F., 2020. Metallic copper removal optimization from real wastewater using pulsed electrodeposition. Journal of hazardous materials 384, 121416.

DesMarais, T.L., Costa, M., 2019. Mechanisms of Chromium-Induced Toxicity. Current opinion in toxicology 14, 1-7.

Dey, S., Paul, A.K., 2012. Optimization of cultural conditions for growth associated chromate reduction by *Arthrobacter sp.* SUK 1201 isolated from chromite mine overburden. Journal of hazardous materials 213-214, 200-206.

Diao, Z., Du, J., Jiang, D., Kong, L., Huo, W., Liu, C., Wu, Q., Xu, X., 2018. Insights into the simultaneous removal of Cr^{6+} and Pb^{2+} by a novel sewage sludge-derived biochar immobilized nanoscale zero valent iron: Coexistence effect and mechanism. The Science of the total environment 642, 505-515.

Diao, Z., Xu, X., Jiang, D., Kong, L., Sun, Y., Hu, Y., Hao, Q., Chen, H., 2016. Bentonite-supported nanoscale zero-valent iron/persulfate system for the simultaneous removal of Cr(VI) and phenol from aqueous solutions. Chemical Engineering Journal 302, 213-222.

Dong, F., Yan, L., Zhou, X., Huang, S., Liang, J., Zhang, W., Guo, Z., Guo, P., Qian, W., Kong, L., Chu, W., Diao, Z., 2021. Simultaneous adsorption of Cr(VI) and phenol by biochar-based iron oxide composites in water: Performance, kinetics and mechanism. Journal of hazardous materials 416, 125930.

Fan, G., Lin, X., You, Y., Du, B., Li, X., Luo, J., 2022. Magnetically separable $ZnFe_2O_4/Ag_3PO_4/g\text{-}C_3N_4$ photocatalyst for inactivation of *Microcystis aeruginosa*: characterization, performance and mechanism. Journal of hazardous materials 421, 126703.

Girelli, A.M., Astolfi, M.L., Scuto, F.R., 2020. Agro-industrial wastes as potential carriers for enzyme immobilization: A review. Chemosphere 244, 125368.

Han, H., Buss, W., Zheng, Y., Song, P., Khalid, R., M., Liu, P., Mašek, O., Li, X., 2022. Contaminants in biochar and suggested mitigation measures – a review. Chemical Engineering Journal 429, 132287.

Han, H., Ling, Z., Zhou, T., Xu, R., He, Y., Liu, P., Li, X., 2017. Copper (II) binding of NAD(P)H- flavin oxidoreductase (NfoR) enhances its Cr (VI)-reducing ability. Scientific reports 7(1), 15481.

Han, H., Rafiq, M.K., Zhou, T., Xu, R., Masek, O., Li, X., 2019. A critical review of clay-based composites with enhanced adsorption performance for metal and organic pollutants. Journal of hazardous materials 369, 780-796.

Han, H., Zheng, Y., Zhou, T., Liu, P., Li, X., 2021. Cu(II) nonspecifically binding chromate reductase NfoR promotes Cr(VI) reduction. Environmental microbiology 23(1), 415-430.

He, C., Zhang, B., Jiang, Y., Liu, H., Zhao, H., 2021. Microbial electrolysis cell produced biogas as sustainable electron donor for microbial chromate reduction. Chemical Engineering Journal 403, 126429.

He, L., Yang, Y., Kim, J., Yao, L., Dong, X., Li, T., Piao, Y., 2020. Multi-layered enzyme coating on highly conductive magnetic biochar nanoparticles for bisphenol A sensing in water. Chemical Engineering Journal 384, 123276.

He, Z., Gao, F., Sha, T., Hu, Y., He, C., 2009. Isolation and characterization of a Cr(VI)-reduction *Ochrobactrum sp.* strain CSCr-3 from chromium landfill. Journal of hazardous materials 163(2-3), 869-873.

Hora, A., Shetty, V.K., 2015. Partial purification and characterization of chromate reductase of a novel *Ochrobactrum sp.* strain Cr-B4. Preparative biochemistry & biotechnology 45(8), 769-784.

Hu, L., Liu, B., Li, S., Zhong, H., He, Z., 2021. Study on the oxidative stress and transcriptional level in Cr(VI) and Hg(II) reducing strain Acinetobacter indicus yy-1 isolated from chromium-contaminated soil. Chemosphere 269, 128741.

Hu, Y., Dai, L., Liu, D., Du, W., Wang, Y., 2018. Progress & prospect of metal-organic frameworks (MOFs) for enzyme immobilization (enzyme/MOFs). Renewable and Sustainable Energy Reviews 91, 793-801.

Huang, D., Zhang, Q., Zhang, C., Wang, R., Deng, R., Luo, H., Li, T., Li, J., Chen, S., Liu, C., 2020. Mn doped magnetic biochar as persulfate activator for the degradation of tetracycline. Chemical Engineering Journal 391, 123532.

Huang, X., Min, D., Liu, D., Cheng, L., Qian, C., Li, W., Yu, H.Q., 2019. Formation mechanism of organo-chromium (III) complexes from bioreduction of chromium (VI) by *Aeromonas hydrophila*. Environment international 129, 86-94.

Imam, A., Suman, S.K., Singh, R., Vempatapu, B.P., Ray, A., Kanaujia, P.K., 2021. Application of laccase immobilized rice straw biochar for anthracene degradation. Environmental pollution 268(Pt A), 115827.

Kourilova, X., Novackova, I., Koller, M., Obruca, S., 2021. Evaluation of mesophilic Burkholderia sacchari, thermophilic Schlegelella thermodepolymerans and halophilic Halomonas halophila for polyhydroxyalkanoates production on model media mimicking lignocellulose hydrolysates. Bioresource technology 325, 124704.

Kumar, A., Park, G. D., Patel, S. K., Kondaveeti, S., Otari, S., Anwar, M. Z., ... & Lee, J. K, 2019. SiO_2 microparticles with carbon nanotube-derived mesopores as an efficient support for enzyme immobilization. Chemical Engineering Journal 359, 1252-1264.

Li, B., Liao, P., Xie, L., Li, Q., Pan, C., Ning, Z., Liu, C., 2020. Reduced NOM triggered rapid Cr(VI) reduction and formation of NOM-Cr(III) colloids in anoxic environments. Water research 181, 115923.

Liu, S., Zeng, G., Niu, Q., Liu, Y., Zhou, L., Jiang, L., Tan, X., Xu, P., Zhang, C., Cheng, M., 2017. Bioremediation mechanisms of combined pollution of PAHs and heavy metals by bacteria and fungi: A mini review. Bioresource technology 224, 25-33.

Lonappan, L., Liu, Y., Rouissi, T., Brar, S.K., Verma, M., Surampalli, R.Y., 2018. Adsorptive immobilization of agro-industrially produced crude laccase on various micro-biochars and degradation of diclofenac. The Science of the total environment 640-641, 1251-1258.

Lonappan, L., Liu, Y., Rouissi, T., Pourcel, F., Brar, S. K., Verma, M., & Surampalli, R. Y., 2018. Covalent immobilization of laccase on citric acid functionalized micro-biochars derived from different feedstock and removal of diclofenac. Chemical Engineering Journal 351, 985-994.

Lu, H., Yan, M., Wong, M.H., Mo, W.Y., Wang, Y., Chen, X.W., Wang, J.J., 2020.

Effects of biochar on soil microbial community and functional genes of a landfill cover three years after ecological restoration. The Science of the total environment 717, 137133.

Luo, J., Lin, L., Liu, C., Jia, C., Chen, T., Yang, Y., Shen, M., Shang, H., Zhou, S., Huang, M., Wang, Y., Zhou, D., Fan, J., Clark, J.H., Zhang, S., Zhu, X., 2020. Reveal a hidden highly toxic substance in biochar to support its effective elimination strategy. Journal of hazardous materials 399, 123055.

Ma, L., Chen, N., Feng, C., 2021. Performance and enhancement mechanism of corncob guiding chromium (VI) bioreduction. Water research 197, 117057.

Mengke, L., Yuting, Z., Yuting, H., Shuzhen, L., Liang, H., Hui, Z., Zhiguo, H., 2019. Exploration on the bioreduction mechanism of Cr(VI) by a gram-positive bacterium: *Pseudochrobactrum saccharolyticum* W1. Ecotoxicology and environmental safety 184, 109636.

Mo, H., Qiu, J., Yang, C., Zang, L., Sakai, E., Chen, J., 2020. Porous biochar/chitosan composites for high performance cellulase immobilization by glutaraldehyde. Enzyme and microbial technology 138, 109561.

Mohamed, A., Yu, L., Fang, Y., Ashry, N., Riahi, Y., Uddin, I., Dai, K., Huang, Q., 2020. Iron mineral-humic acid complex enhanced Cr(VI) reduction by *Shewanella oneidensis* MR-1. Chemosphere 247, 125902.

Naghdi, M., Taheran, M., Brar, S.K., Kermanshahi-Pour, A., Verma, M., Surampalli, R.Y., 2017. Immobilized laccase on oxygen functionalized nanobiochars through mineral acids treatment for removal of carbamazepine. The Science of the total environment 584-585, 393-401.

Shakerian, F., Zhao, J., Li, S.P., 2020. Recent development in the application of immobilized oxidative enzymes for bioremediation of hazardous micropollutants - A review. Chemosphere 239, 124716.

Tan, H., Wang, C., Zeng, G., Luo, Y., Li, H., Xu, H., 2020. Bioreduction and biosorption of Cr(VI) by a novel *Bacillus sp.* CRB-B1 strain. Journal of hazardous materials 386, 121628.

Tang, Z., Kong, Y., Zhao, S., Jia, H., Vione, D., Kang, Y., Gao, P., 2021. Enhancement of Cr(VI) decontamination by irradiated sludge biochar in neutral conditions: Evidence of a possible role of persistent free radicals. Separation and Purification Technology 277, 119414.

Wang, X., Xu, J., Liu, J., Liu, J., Xia, F., Wang, C., Dahlgren, R.A., Liu, W., 2020. Mechanism of Cr(VI) removal by magnetic greigite/biochar composites. The Science of the total environment 700, 134414.

Wen, J., Xue, Z., Yin, X., Wang, X., 2022. Insights into aqueous reduction of Cr(VI) by biochar and its iron-modified counterpart in the presence of organic acids. Chemosphere 286, 131918.

Wu, H., Wang, W., Huang, Y., Han, G., Yang, S., Su, S., Sana, H., Peng, W., Cao, Y., Liu, J., 2019. Comprehensive evaluation on a prospective precipitation-flotation process for metal-ions removal from wastewater simulants. Journal of hazardous

materials 371, 592-602.
Wu, J., Wu, C., Zhou, C., Dong, L., Liu, B., Xing, D., Yang, S., Fan, J., Feng, L., Cao, G., You, S., 2020. Fate and removal of antibiotic resistance genes in heavy metals and dye co-contaminated wastewater treatment system amended with beta-cyclodextrin functionalized biochar. The Science of the total environment 723, 137991.
Wu, M., Li, Y., Li, J., Wang, Y., Xu, H., Zhao, Y., 2019. Bioreduction of hexavalent chromium using a novel strain CRB-7 immobilized on multiple materials. Journal of hazardous materials 368, 412-420.
Xu, X., Huang, H., Zhang, Y., Xu, Z., Cao, X., 2019. Biochar as both electron donor and electron shuttle for the reduction transformation of Cr(VI) during its sorption. Environmental pollution 244, 423-430.
Xu, X., Pose-Boirazian, T., Eibes, G., McCoubrey, L.E., Martínez-Costas, J., Gaisford, S., Goyanes, A., Basit, A.W., 2021. A customizable 3D printed device for enzymatic removal of drugs in water. Water research.
Yan, L., Dong, F., Lin, X., Zhou, X., Kong, L., Chu, W., Diao, Z., 2021. Insights into the removal of Cr(VI) by a biochar‐iron composite from aqueous solution: Reactivity, kinetics and mechanism. Environmental Technology & Innovation 24.
Yang, Q., Yan, Y., Yang, X., Liao, G., Wang, D., Xia, H., 2019. Enzyme immobilization in cage-like 3D-network PVA-H and GO modified PVA-H (GO@PVA-H) with stable conformation and high activity. Chemical Engineering Journal 372, 946-955.
Yang, W., Xi, D., Li, C., Yang, Z., Lin, Z., Si, M., 2021. "In-situ synthesized" iron-based bimetal promotes efficient removal of Cr(VI) in by zero-valent iron-loaded hydroxyapatite. Journal of hazardous materials 420, 126540.
Ye, S., Cheng, M., Zeng, G., Tan, X., Wu, H., Liang, J., Shen, M., Song, B., Liu, J., Yang, H., Zhang, Y., 2020. Insights into catalytic removal and separation of attached metals from natural-aged microplastics by magnetic biochar activating oxidation process. Water research 179, 115876.
Yi, Y., Huang, Z., Lu, B., Xian, J., Tsang, E.P., Cheng, W., Fang, J., Fang, Z., 2020a. Magnetic biochar for environmental remediation: A review. Bioresource technology 298, 122468.
Yi, Y., Tu, G., Tsang, P.E., Fang, Z., 2020b. Insight into the influence of pyrolysis temperature on Fenton-like catalytic performance of magnetic biochar. Chemical Engineering Journal 380, 122518.
Yi, Y., Tu, G., Zhao, D., Tsang, P.E., Fang, Z., 2020c. Key role of FeO in the reduction of Cr(VI) by magnetic biochar synthesised using steel pickling waste liquor and sugarcane bagasse. Journal of Cleaner Production 245, 118886.
Yin, Z., Liu, Y., Liu, S., Jiang, L., Tan, X., Zeng, G., Li, M., Liu, S., Tian, S., Fang, Y., 2018. Activated magnetic biochar by one-step synthesis: Enhanced adsorption and coadsorption for 17beta-estradiol and copper. The Science of the total environment 639, 1530-1542.
Younas, F., Niazi, N.K., Bibi, I., Afzal, M., Hussain, K., Shahid, M., Aslam, Z., Bashir, S., Hussain, M.M., Bundschuh, J., 2021. Constructed wetlands as a sustainable

technology for wastewater treatment with emphasis on chromium-rich tannery wastewater. Journal of hazardous materials 422, 126926.
Zeng, Q., Hu, Y., Yang, Y., Hu, L., Zhong, H., He, Z., 2019. Cell envelop is the key site for Cr() reduction by *Oceanobacillus oncorhynchi* W4, a newly isolated Cr(VI) reducing bacterium. Journal of hazardous materials 368, 149-155.
Zhang, H., Hay, A.G., 2020. Magnetic biochar derived from biosolids via hydrothermal carbonization: Enzyme immobilization, immobilized-enzyme kinetics, environmental toxicity. Journal of hazardous materials 384, 121272.
Zhang, R., Li, Y., Wang, Z., Tong, Y., Sun, P., 2020. Biochar-activated peroxydisulfate as an effective process to eliminate pharmaceutical and metabolite in hydrolyzed urine. Water research 177, 115809.
Zhang, T., Chen, J., Xiong, H., Yuan, Z., Zhu, Y., Hu, B., 2021. Constructing new Fe_3O_4@MnO_x with 3D hollow structure for efficient recovery of uranium from simulated seawater. Chemosphere 283, 131241.
Zhang, Y., Piao, M., He, L., Yao, L., Piao, T., Liu, Z., Piao, Y., 2020. Immobilization of laccase on magnetically separable biochar for highly efficient removal of bisphenol A in water. RSC Advances 10(8), 4795-4804.
Zhong, D., Zhang, Y., Wang, L., Chen, J., Jiang, Y., Tsang, D.C.W., Zhao, Z., Ren, S., Liu, Z., Crittenden, J.C., 2018. Mechanistic insights into adsorption and reduction of hexavalent chromium from water using magnetic biochar composite: Key roles of Fe_3O_4 and persistent free radicals. Environmental pollution 243, 1302-1309.
Zhu, S., Huang, X., Yang, X., Peng, P., Li, Z., Jin, C., 2020. Enhanced transformation of Cr(VI) by heterocyclic-N within nitrogen-doped biochar: impact of surface modulatory persistent free radicals (PFRs). Environmental science & technology 54(13), 8123-8132.

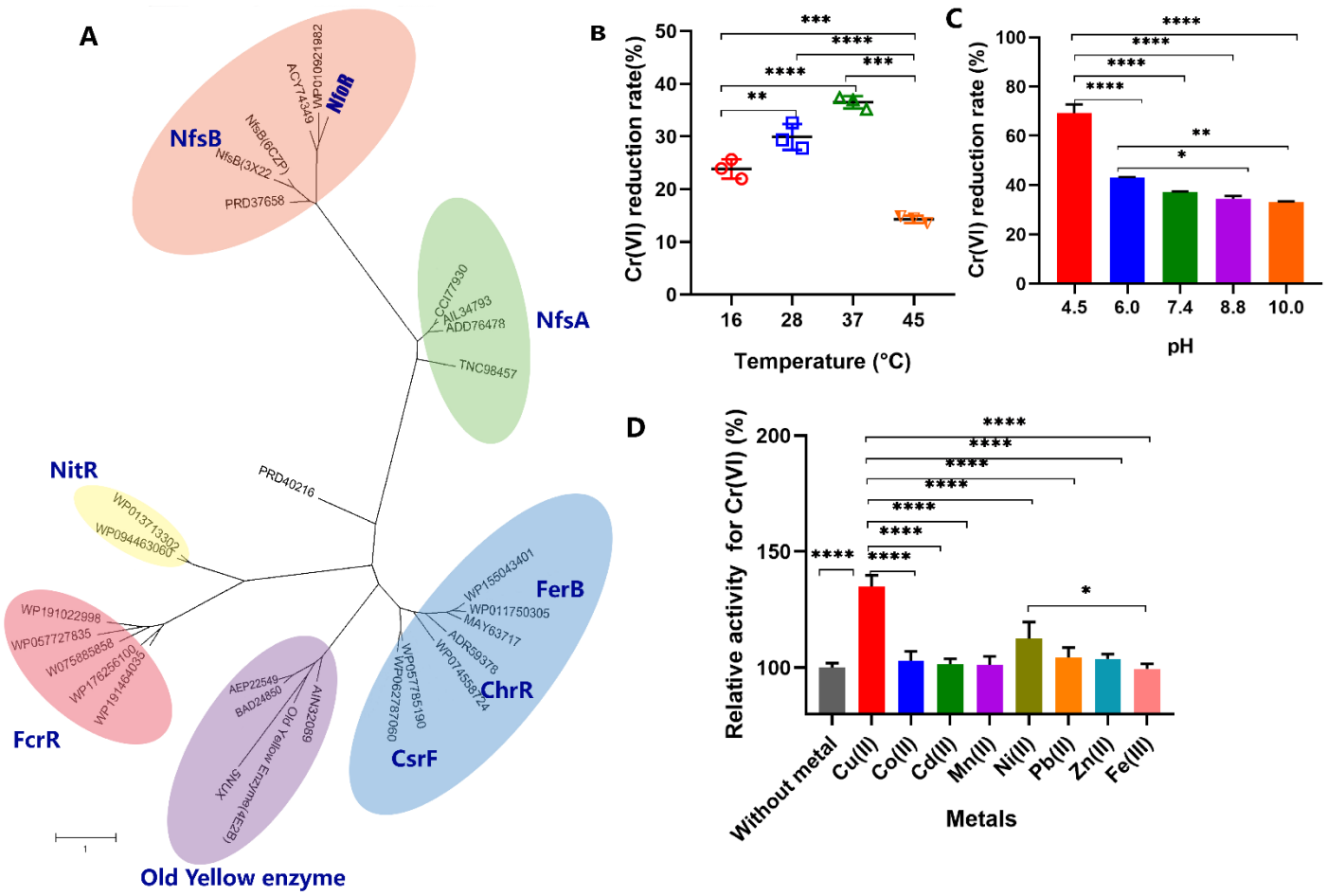

Fig. 1 A, Unrooted phylogenetic tree of known chromate reductase. The GenBank or PDB code are shown at the leaves; B-D, Effects of pH (B), temperature (C), and various heavy metals on NfoR activity (D). * *P*<0.05, ** *P*<0.01, * *P*<0.001.**

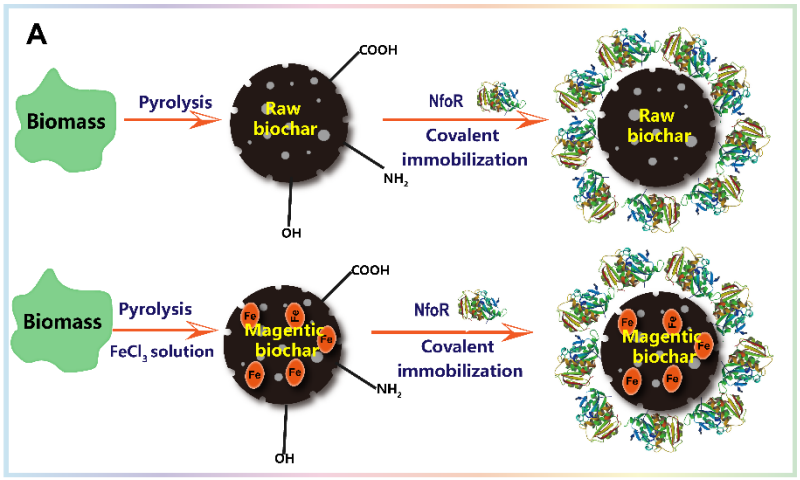
A
Biomass
Pyrolysis
Raw biochar
COOH
NH2
OH
NfoR
Covalent immobilization
Raw biochar
Biomass
Pyrolysis
FeCl3 solution
Magentic biochar
Fe
COOH
NH2
OH
NfoR
Covalent immobilization
Magentic biochar

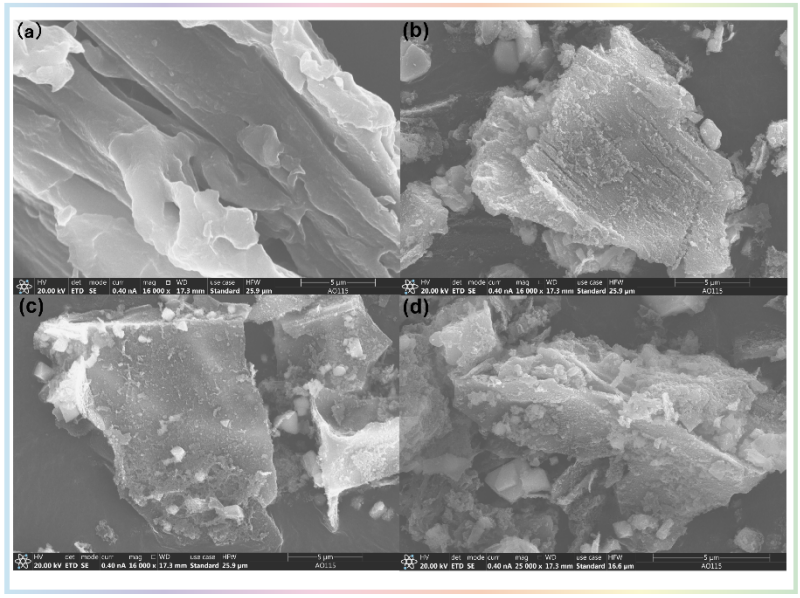
B
(a)
(b)
(c)
(d)

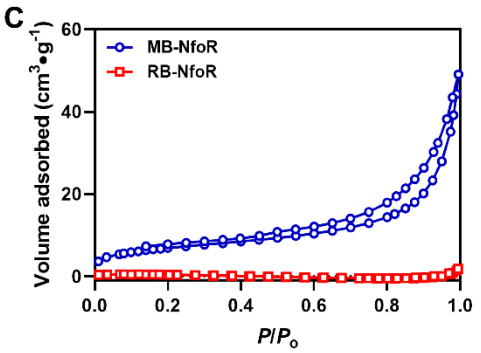
C
MB-NfoR
RB-NfoR
Volume adsorbed (cm3•g-1)
P/Po
0
20
40
60
0.0
0.2
0.4
0.6
0.8
1.0

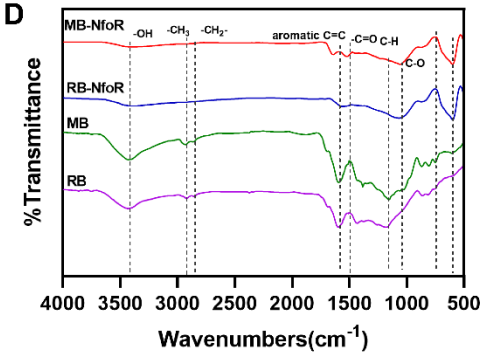
D
MB-NfoR
-OH
-CH3
-CH2-
aromatic C=C
-C=O C-H
C-O
RB-NfoR
MB
RB
%Transmittance
4000 3500 3000 2500 2000 1500 1000 500
Wavenumbers(cm-1)

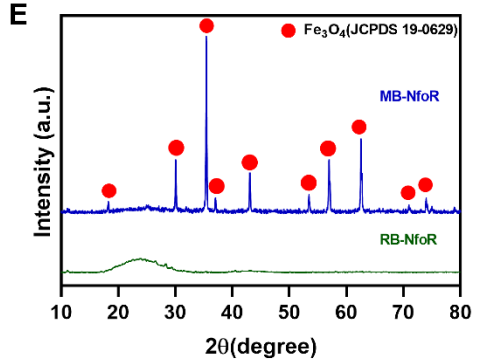
E
Fe3O4(JCPDS 19-0629)
MB-NfoR
RB-NfoR
Intensity (a.u.)
10 20 30 40 50 60 70 80
2θ(degree)

Fig. 2 A, Schematics of chromate reductase NfoR immobilized on magnetic biochar and raw biochar via 3% glutaraldehyde crosslinking; B, SEM images of raw biochar (RB), magnetic biochar (MB), raw biochar-immobilized NfoR (RB-NfoR), and magnetic biochar-immobilized NfoR (MB-NfoR), respectively; C, N_2 adsorption isotherms of immobilized NfoR; D, FTIR spectra of RB, MB, RB-NfoR, and MB-NfoR; E, XRD patterns of MB-NfoR and RB-NfoR.

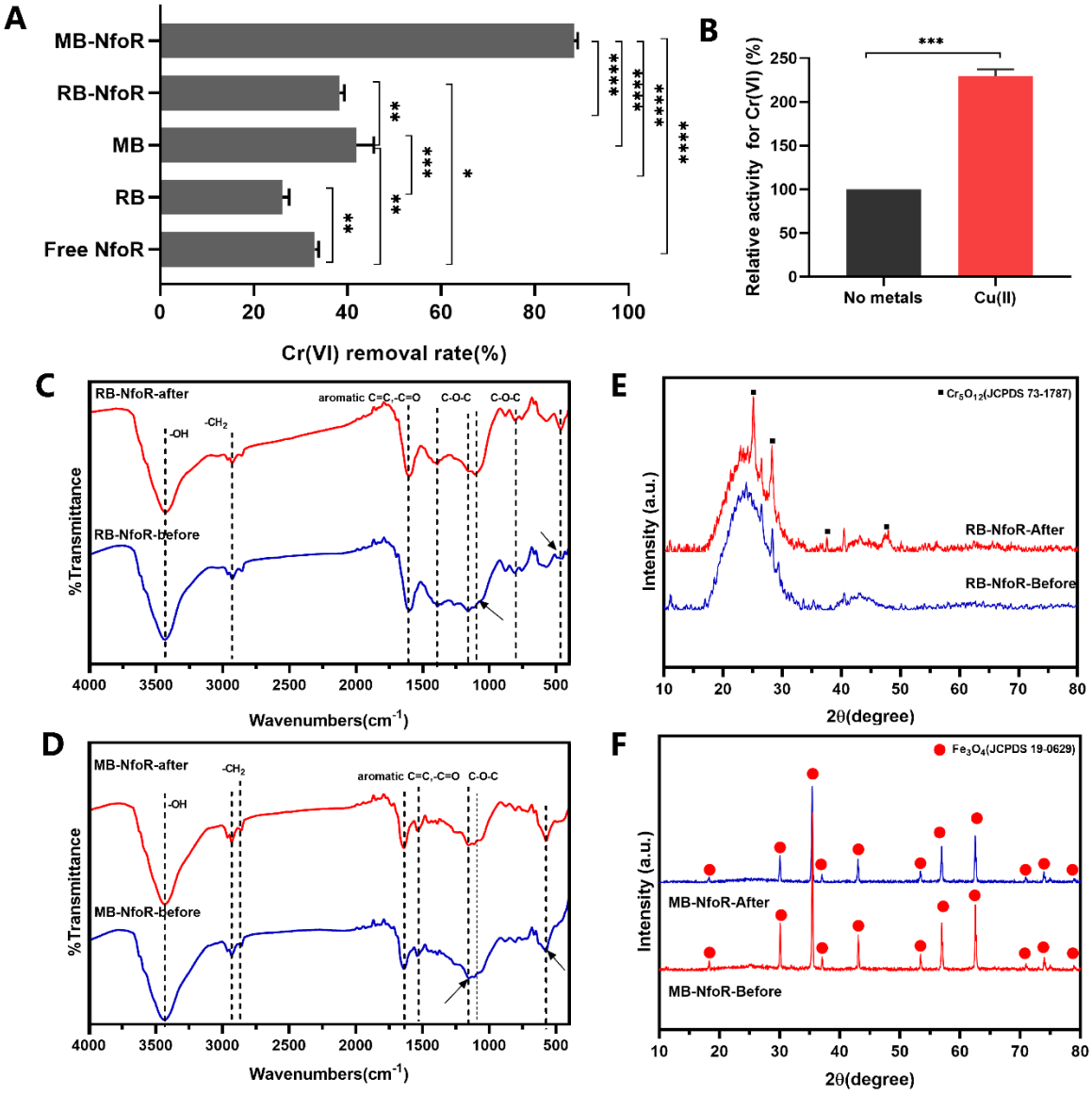

Fig. 3 A, Cr(VI) removal rate of free enzyme NfoR, raw biochar (RB), magnetic biochar (MB), RB-NfoR, and MB-NfoR; B, the presence of Cu(II) enhanced the relative activity of MB-NfoR; C, D, The FTIR spectra of RB-NfoR (C) and MB-NfoR (D) before and after reaction; E, F, XRD patterns of RB-NfoR (E) and MB-NfoR (F) before and after reaction. asterisk means significant difference between different treatments. * *P*<0.05, ** *P*<0.01, * *P*<0.001**

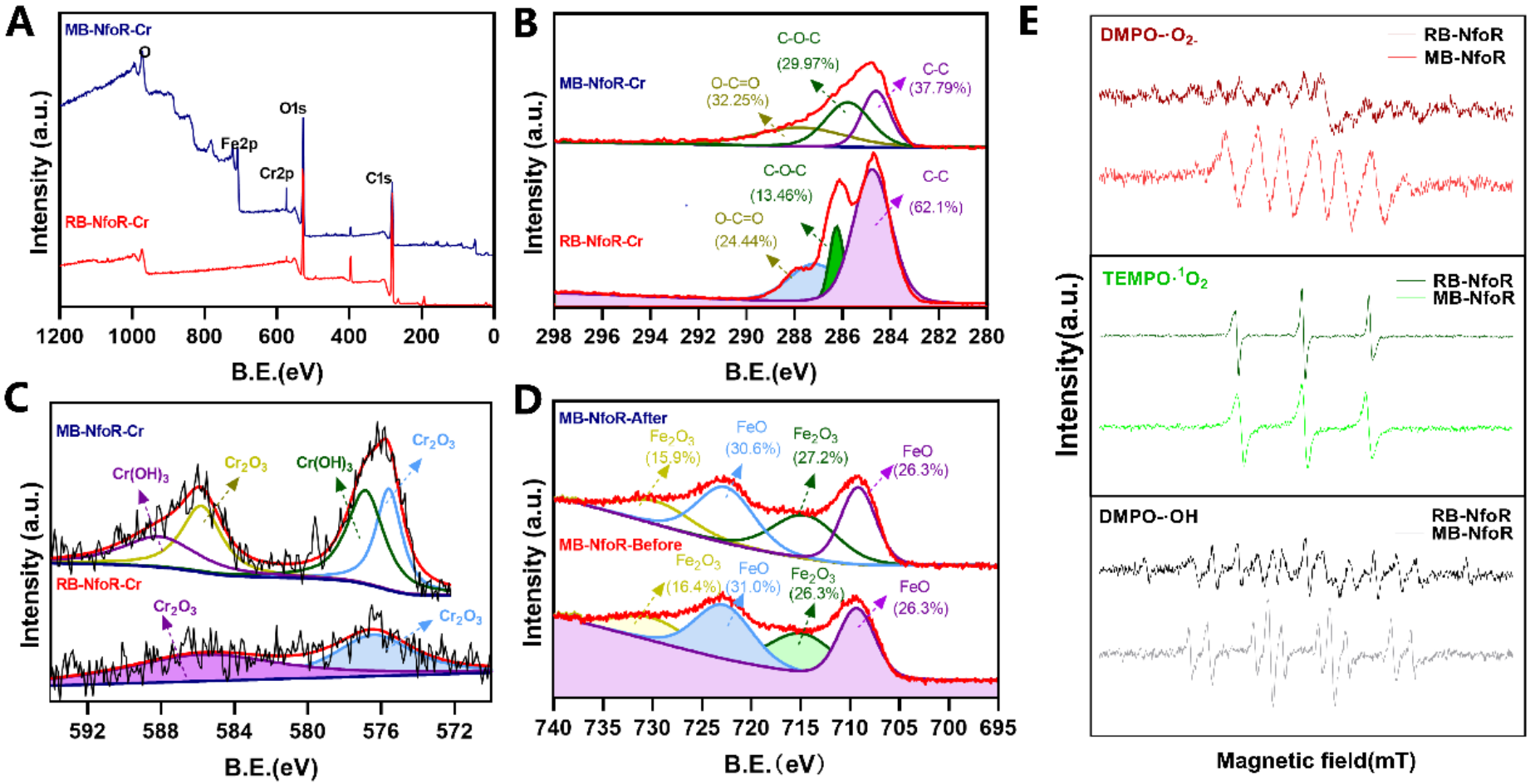

Fig. 4 XPS spectra of RB-NfoR and MB-NfoR after Cr(VI) removal. A, The total survey spectra; B, C and D, high resolution of C1s, Cr_{2p}, Fe_{2p}, respectively; E, EPR spectra of DMPO-•OH, DMPO-•O_{2-} and TEMPO-$^1O_2$ derived from RB-NfoR and MB-NfoR systems.

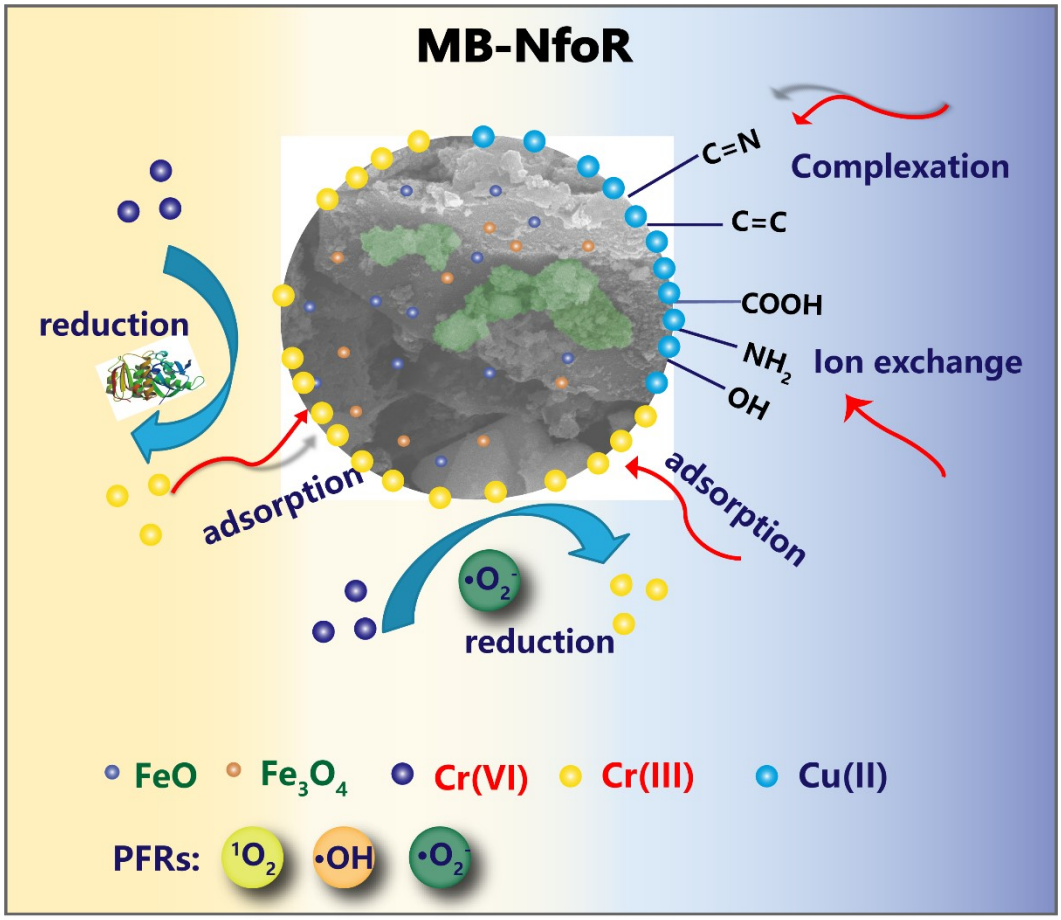

Fig. 5 Proposed Cr(VI) and Cu(II) removal mechanism of MB-NfoR.

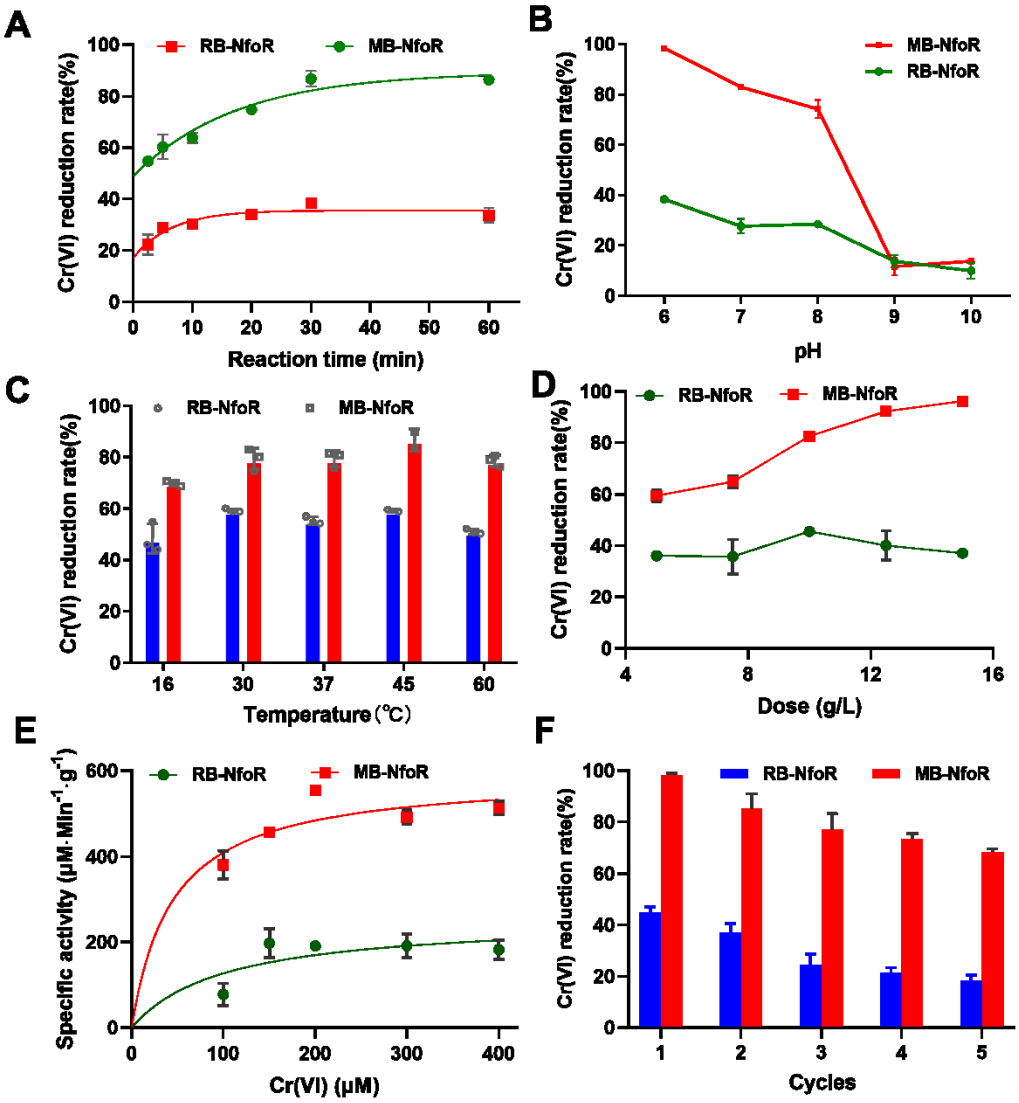

Fig. 6 Performance optimization of immobilized NfoR under various parameters. A, reaction time; B, pH change; C, temperature; D, dose of immobilized NfoR; E, initial Cr(VI) concentration; F, regeneration of RB-NfoR and MB-NfoR after five consecutive cycles. The Fig. 6E was fitted with Michaelis–Menten equation for evaluating immobilized-enzyme kinetics. Experimental conditions: initial pH = 7.0, C_0 = 0.2 M·L^{-1}, and dosage = 10 g·L^{-1}.

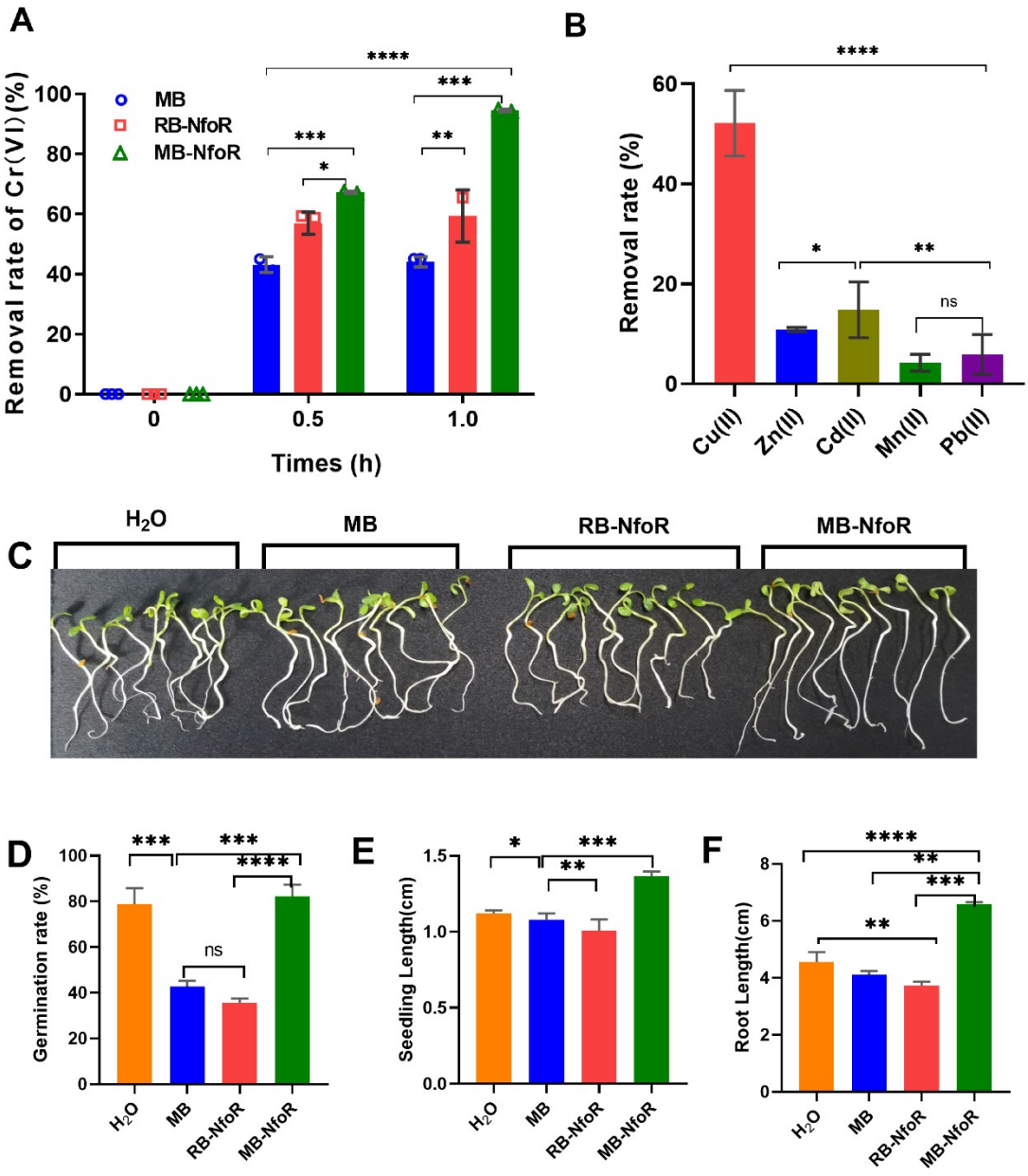

Fig. 7A, Cr(VI) removal of smelting wastewater by MB, RB-NfoR, and MB-NfoR; B, adsorption removal of other divalent ions in smelting wastewater via MB-NfoR; C, germination and growth of alfalfa after exposure to treated smelting wastewater by MB and biochar-immobilized NfoR for five days. D, germination rate; E, seedling length; F, root length. * *P*<0.05, ** *P*<0.01, * *P*<0.001, **** *P*<0.0001, and ns indicates no significant difference.**

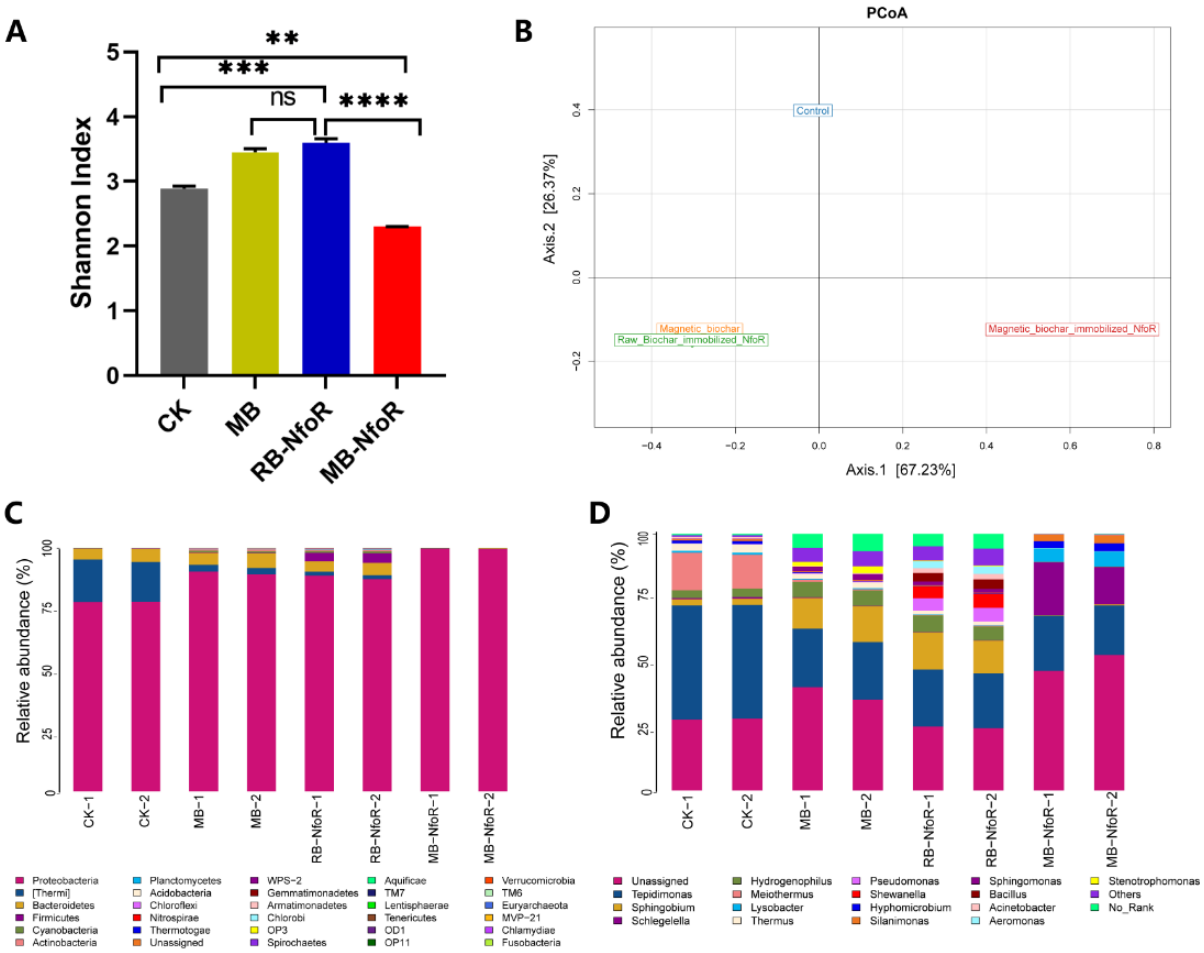

Fig. 8 Different immobilized NfoR shifts the microbial structure of smelting wastewater (A) α-diversity of each sample as measured by the Shannon diversity index. (B) Scatter plot of the principal coordinate analysis (PcoA) scores depicting variance in the microflora of smelting wastewater. (C, D) Relative bacterial abundance in smelting wastewater at the phylum and genus levels. The CK group represents smelting wastewater, whereas MB, RB-NfoR, and MB-NfoR represent wastewater treated by magnetic biochar, raw biochar-immobilized NfoR, and magnetic biochar-immobilized NfoR.

Table 1 Performance of various biochar-immobilized enzymes from this and other studies.

Enzyme	Support	Immobilization methods	Cycles	Residual activity	References
Laccase Horse radish peroxidase	Magnetic biochar from sludge	Adsorption	10	79% 60%	(Zhang and Hay, 2020)
Laccase	rice straw biochar	Adsorption	6	60%	(Imam et al., 2021)
Laccase	Acid activated biochar from Pig manure, pine wood and almond shell	Covalent immobilization	5	40%-46%	(Lonappan, 2018)
Laccase	Pinewood biochar	Adsorption	7	6%	(Naghdi et al., 2017)
Laccase	Magnetic biochar	Covalent immobilization	7	85%	(Zhang, Y. et al., 2020)
Cellulase	Bagasse biochar/chitosan composites	Covalent immobilization	10	90-69%	(Mo et al., 2020)
Chromate reductase	Magnetic biochar from pine sawdust	Covalent immobilization	5	68.3%	This study